

Physical Properties of Photonic Cooper Pairs Generated via Correlated Stokes–anti-Stokes Raman Scattering

Filomeno S. de Aguiar Júnior, Carlos H. Monken, Marcelo F. Santos, Reinaldo de Melo e Souza, André Saraiva, Belita Koiller, and Ado Jorio*

The theoretical and experimental background for the creation of photonic Cooper pairs (PCPs) via correlated Stokes–anti-Stokes Raman scattering is introduced, followed by experimental results on the second-order photon time correlation $g^2(0)$ in diamond. It is shown how $g^2(0)$ changes with energy (Stokes–anti-Stokes Raman shift), momentum (scattering angle) and excitation laser power. Both real and virtual phonon-mediated scattering processes are addressed.

1. Introduction

Anomalous Stokes to anti-Stokes ratio in the radial breathing mode Raman scattering in isolated single-wall carbon nanotubes was observed early in 2001. The resonance window for the anti-Stokes signal appeared overall more intense than the resonance window for the Stokes signal.^[1] Interestingly, these results triggered the studies of correlated Stokes–anti-Stokes phenomenon in graphene,^[2] while later on the carbon nanotube results were explained as a consequence of Raman processes that includes the phonon-mediated interactions with dark excitonic states^[3] and correlated Stokes–anti-Stokes processes in carbon nanotubes have not been demonstrated so far.

Consequently, the anti-Stokes (aS) to Stokes (S) intensity ratio (I_{aS}/I_S) in Raman scattering has been generalized to account for correlated Stokes–anti-Stokes (SaS) scattering,^[4] approximated by^[5]

$$\frac{I_{aS}}{I_S} = C' \left(\frac{n_0}{n_0 + 1} + f_{SaS} P_L \right) \quad (1)$$

where the function f_{SaS} measures the importance of the SaS phenomena, P_L is the excitation laser power, n_0 is the Bose–Einstein distribution function, and C' depends on the optical properties of the sample and instrumental apparatus.

Equation (1) is valid in resonance with the vibrational transition, i.e., $I_{S,aS}$ is measured at energies matching the S,aS vibrational Raman shifts.^[5] This correlated SaS light scattering phenomenon involving the exchange of real phonons has been studied recently in diamond^[6–9] and graphene,^[2,8] evidencing a time correlation at zero delay beyond the maximum classical correlation given by the Cauchy–Schwarz inequality, indicating that this phenomenon has no classical analog.

When the energy shift in S or aS is tuned out of resonance with the vibrational level, the process takes place through the exchange of virtual phonons, generating the photonic Cooper pairs (PCPs),^[10–12] an analogous of the Cooper pairs responsible for electronic superconductivity.^[13] These results have been observed not only in diamond and graphene, but also in other transparent media, including liquids.^[10,11,14]

In this paper we briefly discuss the theoretical and experimental background for doing such a Raman experiment in the quantum regime. We present experimental results from diamond, including the SaS dependence on scattering energy, scattering momentum and excitation laser power.

2. Methods

2.1. Theory

The Hamiltonian for the inelastic (Raman) scattering process can be written as $H = H_0 + H_1$. The first term

$$H_0 = \sum_{\mathbf{k}} \hbar \omega_{\mathbf{k}} b_{\mathbf{k}}^{\dagger} b_{\mathbf{k}} + \sum_{\mathbf{q}} \hbar \nu_{\mathbf{q}} c_{\mathbf{q}}^{\dagger} c_{\mathbf{q}} \quad (2)$$


describes the electromagnetic and the material vibration free Hamiltonian (neglecting the zero point energy, which will not affect our results), composed by photons with energy $\hbar \omega_{\mathbf{k}}$ and phonons with energy $\hbar \nu_{\mathbf{q}}$. The q is in general an index of the vibrational mode involved. In the particular case of crystals, it is

F. S. de Aguiar Júnior, Prof. C. H. Monken, Prof. A. Jorio
Departamento de Física, UFMG
Belo Horizonte MG 31270-901, Brazil
E-mail: adojorio@fisica.ufmg.br

Prof. M. F. Santos, Prof. A. Saraiva, Prof. B. Koiller
Instituto de Física, UFRJ
CP 68528, Rio de Janeiro, RJ 21941-972, Brazil

Prof. R. de Melo e Souza
Instituto de Física, UFF
Niterói, RJ 24210-346, Brazil

Prof. A. Saraiva
Centre for Quantum Computation and Communication Technology
School of Electrical Engineering and Telecommunications
The University of New South Wales
Sydney, NSW 2052, Australia

 The ORCID identification number(s) for the author(s) of this article can be found under <https://doi.org/10.1002/pssb.201900218>.

DOI: 10.1002/pssb.201900218

the optical phonon momentum. The b_k^\dagger and c_q^\dagger are the dimensionless creation operators for photon and phonons, respectively. The second term

$$H_1 = \sum_{k,q} M_q (c_q^\dagger + c_{-q}) b_k b_{k-q}^\dagger \quad (3)$$

describes the light–matter interaction, where the $c_q^\dagger b_k b_{k-q}^\dagger$ term generates scattered photons with the concomitant creation of a phonon (via the so-called Stokes process), and the $c_{-q} b_k b_{k-q}^\dagger$ term generates scattered photons with the concomitant annihilation of a phonon (via the so-called anti-Stokes process).^[5,10]

Through a similarity transformation,^[15] it can be shown that the Hamiltonian H_1 is equivalent to a simpler one that in the limit of low number of phonons and weak coupling becomes^[10]

$$H_1' = \sum_{k,k',q} \frac{M_q^2 \nu_q}{\hbar [(\omega_k - \omega_{k-q})^2 - \nu_q^2]} b_{k-q}^\dagger b_{k'+q}^\dagger b_k b_{k'} \quad (4)$$

which is analogous to the BCS interaction Hamiltonian.^[10,13]

The b operators here are bosons (photons) while in BCS they are fermions (electrons), in which case the existence of a Fermi sphere leads to a transition to the superconducting state at low enough temperatures. The analogy presented here is formally related to the formation of PCPs. No superconducting state is theoretically anticipated.

Weak coupling in this context means

$$\|M_q\| \ll \|\hbar(\omega_k - \omega_{k-q} \pm \nu_q)\| \quad (5)$$

This condition is in general met since the photon–phonon coupling for visible light is a higher order process mediated by the virtual creation of electron–hole pairs, which emits or absorbs a phonon and recombines. Since the right hand side of Equation (5) is of the order of tens of meV, this condition is only broken at a very narrow band around the Raman peak, which is beyond our resolution, specially at room temperature and under a femtosecond pulsed laser.

The interaction potential is shown in **Figure 1** by the dashed lines, which diverge when resonance is achieved, i.e., when $(\omega_k - \omega_{k-q}) = \nu_q$. The red line in **Figure 1** is an approximation potential, considered constant $-V_0$ in the region of attractive photon–photon interaction (negative V) and null (no pair formation) in the region of repulsive photon–photon interaction (positive V). This is inspired by the approximations adopted in the BCS model.^[13]

The second-order time correlation between the number of Stokes (n_S) and anti-Stokes (n_{aS}) photons detected at times t and $t' = t + \Delta t$ is defined as

$$g_{S,aS}^{(2)}(\Delta t) = \frac{\langle n_S(t) n_{aS}(t') \rangle}{\langle n_S(t) \rangle \langle n_{aS}(t') \rangle} \quad (6)$$

This quantity is useful to probe the quantum nature of the SaS process. For simultaneously detected photons, $t = t'$, thus $\Delta t = 0$. This is the quantity we measure in our experiments, as discussed in the next sections.

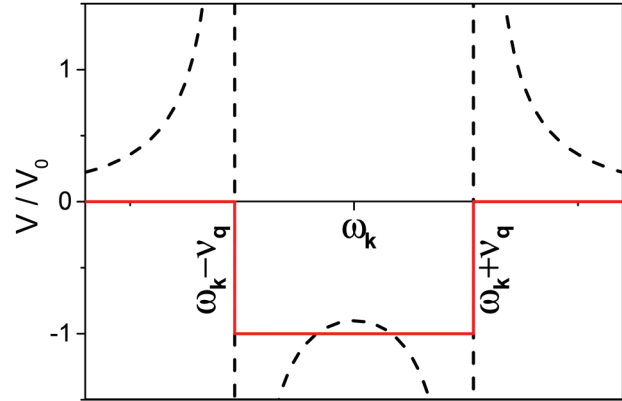


Figure 1. The dashed line shows the interaction potential as given by Equation (4). The red line is an approximation potential, as described in the text. The ω_k gives the excitation laser frequency and ν_q the vibrational frequency.

2.2. Experimental Details

The $g_{S,aS}^{(2)}(\Delta t = 0)$ correlation function can be evaluated experimentally by

$$g_{S,aS}^{(2)}(\Delta t = 0) = \frac{I_{SaS}(\Delta t = 0)}{\bar{I}_{SaS}(\Delta t \neq 0)} \quad (7)$$

where $I_{SaS}(\Delta t = 0)$ is the number of pairs measured in coincidence and $\bar{I}_{SaS}(\Delta t \neq 0)$ is the average over the measured non-coincident SaS count rates $I_{SaS}(\Delta t \neq 0)$.

Figure 2 shows the basic constituents of the experimental apparatus utilized to measure SaS correlated Raman scattering: a pulsed laser excites a sample after passing through a bandpass filter (here a 633 nm laser at 76 MHz rate, 200 fs pulse width); the scattered light is colimated and directed to a spectrometer after passing through a notch filter that removes the laser energy – up to this point the apparatus is very similar to a regular Raman spectrometer; for studying the angular scattering spread, we placed an iris of variable aperture radius (r) 7 cm after the colimation lens (25 cm focal length); for the SaS measurement, however, the spectrometer filters the Stokes and anti-Stokes lines, sending them separately into two photo-counter detectors (avalanche photodiodes, APDs), which are connected to a time correlated single-photon counting system; this time delay detector generates a histogram with the number of SaS pairs as a function of Δt , as shown in the lower-left in **Figure 2**; $I_{SaS}(\Delta t = 0)$ is the height of the central peak, and $\bar{I}_{SaS}(\Delta t \neq 0)$ is the average height over the peaks at $\Delta t \neq 0$; subsequent $\Delta t \neq 0$ peaks are spaced by ≈ 13 ns, consistent with the 76 MHz pulsed excitation.

3. Results and Discussion

SaS-related experimental results obtained in a high purity 1.7 mm-thick diamond slab are discussed here.

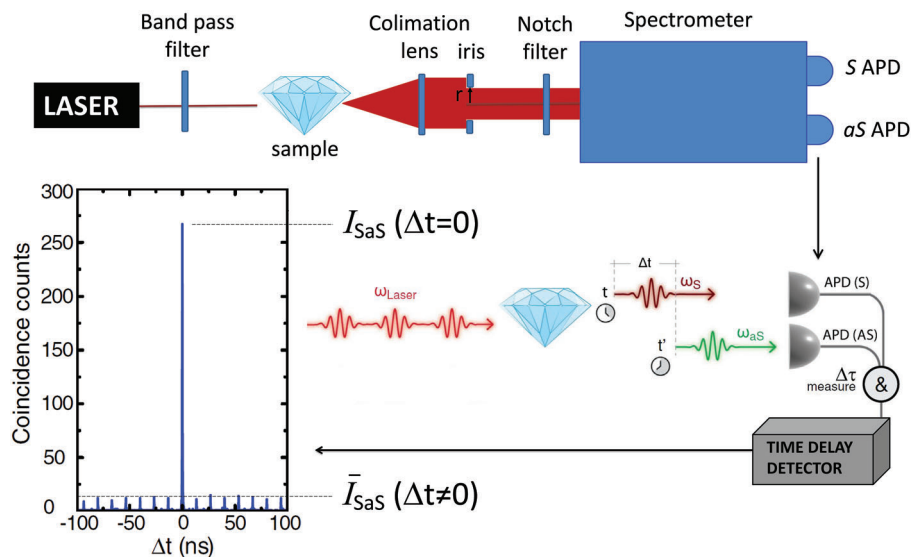


Figure 2. Schematics of the experimental apparatus, showing a simplified version of the setup on top, and the excitation and measurement procedures in the bottom. The graphics on the lower-left is an histogram of SaS measured in diamond, where we indicate the experimentally observed $I_{\text{SaS}}(\Delta t = 0)$ and $\bar{I}_{\text{SaS}}(\Delta t \neq 0)$ values. For more details on the experimental apparatus and measurement, see the Supporting Information in ref. [11].

3.1. Energy Dependence

Figure 3 shows the correlation function $g_{\text{S,aS}}^{(2)}(\Delta t = 0)$ (black circles connected by dashed lines) as a function of the Raman shift modulus (Stokes shift equals to minus anti-Stokes shift). The result is superimposed with the Stokes Raman spectrum (red line) measured with a regular CCD, and with the measured

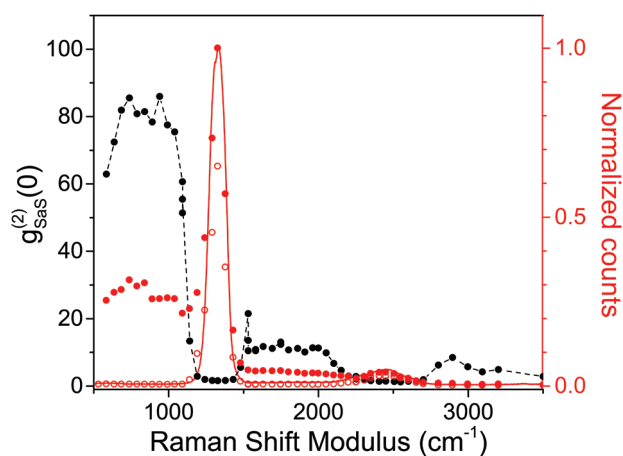


Figure 3. Black circles connected by dashed lines give the $g_{\text{S,aS}}^{(2)}(0)$ dependence on Stokes/anti-Stokes Raman shifts. The red line gives the Stokes Raman spectrum and the solid and open red circles give $I_{\text{SaS}}(\Delta t = 0)$ and $\bar{I}_{\text{SaS}}(\Delta t \neq 0)$, respectively. The Raman spectrum and the $I_{\text{SaS}}(\Delta t = 0)$ data were normalized to their highest values. $\bar{I}_{\text{SaS}}(\Delta t \neq 0)$ was normalized to keep the relative intensity to $I_{\text{SaS}}(\Delta t = 0)$ as observed. This experiment was performed with 44 mW reaching the sample, total accumulation time of 600 s per point, filtering only the Stokes signal with a monochromator of 26 cm^{-1} resolution.

$I_{\text{SaS}}(\Delta t = 0)$ (solid red circles) and $\bar{I}_{\text{SaS}}(\Delta t \neq 0)$ (open red circles) signals. The main peak at 1332 cm^{-1} corresponds to the first-order Raman-allowed C-C vibration in diamond, and the observed peak lineshape (Gaussian) corresponds to the pulsed laser.

Out-of-resonance values of $g_{\text{S,aS}}^{(2)}(\Delta t = 0)$ are typically high, decreasing sharply when the Raman shift approaches a real vibrational energy, both at the first-order (1332 cm^{-1}) and second-order (2450 cm^{-1}) peaks. This result is in agreement with previous observations in water,^[14] and it happens because, in resonance, the number of uncorrelated Stokes and anti-Stokes photons increases significantly, as shown by the red-open circles in Figure 3. The $g_{\text{S,aS}}^{(2)}(\Delta t = 0)$ is highest below the first-order Raman peak at 1332 cm^{-1} , where the SaS rate is maximum (see solid-red circles). Above 1332 cm^{-1} , two-phonons second-order Raman signal is observed and the SaS production rate is highly reduced.^[11]

3.2. Momentum Dependence

To study the scattering angle with respect to the incident light direction, the scattered light has been colimated by a lens and the solid angle of the colimated scattered light limited by an iris of variable radius, as illustrated in Figure 2.^[11]

Figure 4 shows the iris radius (related to the scattering angle) dependence for the correlation function $g_{\text{S,aS}}^{(2)}(\Delta t = 0)$ (top panels), $I_{\text{SaS}}(\Delta t = 0)$ (middle panels), and $\bar{I}_{\text{SaS}}(\Delta t \neq 0)$ (bottom panels) measured in resonance (at 1332 cm^{-1} , left panels) and out of resonance (at 900 cm^{-1} , right panels). The $g_{\text{S,aS}}^{(2)}(\Delta t = 0)$ for the real (resonant) process decays toward the classical value $g_{\text{S,aS}}^{(2)}(\Delta t = 0) = 2$ when the iris is fully open, while the virtual (out-of-resonance) scattering remains basically constant, independent on the iris radius.

The difference between real and virtual SaS can be explained as follows: the truly correlated pairs are highly focused in

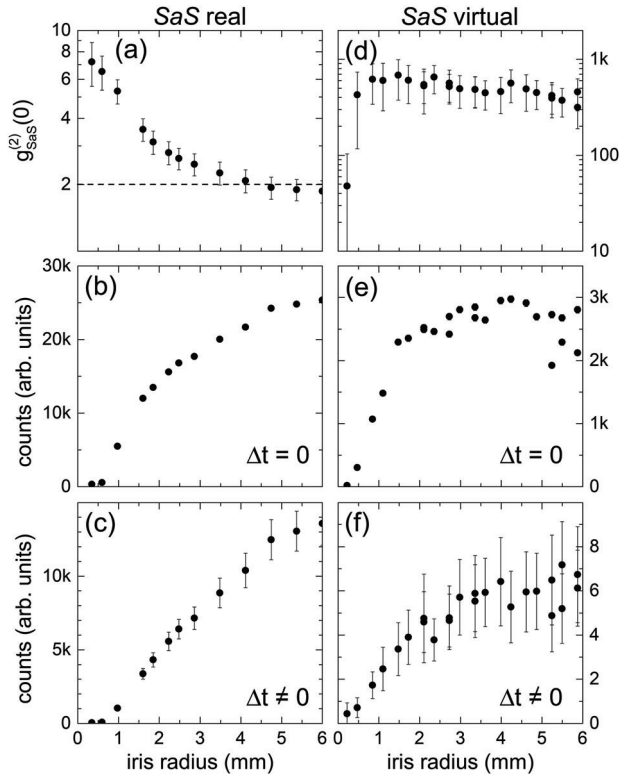


Figure 4. Dependence of $g_{S,aS}^{(2)}(\Delta t = 0)$ (a,d), $I_{S,aS}(\Delta t = 0)$ (b,e), and $\bar{I}_{S,aS}(\Delta t \neq 0)$ (c,f) on the aperture radius of the iris blocking the scattered signal as collected by a colimation lens. The left panels (a–c) stand for the real processes, measured at 1332 cm^{-1} Raman shift, and the right panels (d–f) stand for the virtual processes, measured at 900 cm^{-1} Raman shift. The Y scales are logarithmic in (a,d) and linear in the other panels. The error bars are given by \sqrt{N} , where N is the total number of counts. The error bars cannot be seen when the errors are smaller than the symbols. This experiment was performed with 44 mW reaching the sample, total accumulation time of 600 s per point, filtering the Stokes signal with a monochromator of 26 cm^{-1} resolution. For the virtual process (d–f), a 15 nm broad-band filter was utilized to further filter the aS signal.

forward scattering, i.e., no angular scattering, appearing for iris radii below 2 mm , which is roughly the excitation laser beam diameter; the uncorrelated signal is spread in higher angles due to momentum transfer in the real phonon mediated scattering, so that the $\bar{I}_{S,aS}(\Delta t \neq 0)$ increases significantly in the real process when opening the iris, consequently decreasing the measured $g_{S,aS}^{(2)}(\Delta t = 0)$.

The same behavior does not happen for the virtual process, basically because out of resonance the single source for anti-Stokes photons is the correlated SaS process, which takes place only below 2 mm in iris radius. Therefore, the values of both $I_{S,aS}(\Delta t = 0)$ and $\bar{I}_{S,aS}(\Delta t \neq 0)$ increase and reach their maximum values when the iris is opened up to 2 mm , and from that point on the values remain roughly constant.

Other aspects deserve note: (1) both $I_{S,aS}(\Delta t = 0)$ and $\bar{I}_{S,aS}(\Delta t \neq 0)$ tend to zero when the iris is closed down to $\approx 0.5 \text{ mm}$, instead of going to zero only when the iris is fully closed. This result is most probably due to a slight iris misalignment with respect to the excitation laser beam direction,

besides the fact that in our experiment the iris is not placed on the back focal length of the colimation lens; (2) out of resonance, the number of counts in $I_{S,aS}(\Delta t \neq 0)$ is lesser than one per minute. This count rate limits the amount of acquired data, which sets the large relative errors in panels (d) and (f); (3) out of resonance, the $g_{S,aS}^{(2)}(\Delta t = 0)$ value is very large (when compared to the typical classical value of $g^{(2)} = 2$), similar to the observed in water,^[14] both because of the very low $\bar{I}_{S,aS}(\Delta t \neq 0)$ values when compared with $I_{S,aS}(\Delta t = 0)$.

3.3. Power Dependence

The excitation laser power dependence for $g_{S,aS}^{(2)}(\Delta t = 0)$, $I_{S,aS}(\Delta t = 0)$, and $\bar{I}_{S,aS}(\Delta t \neq 0)$ in the real SaS process in diamond

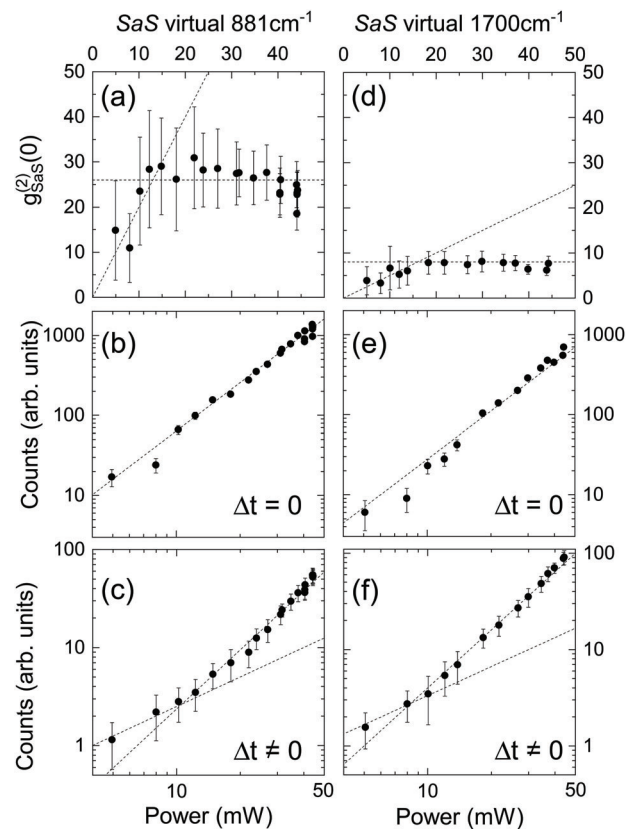


Figure 5. Excitation laser power dependence of $g_{S,aS}^{(2)}(\Delta t = 0)$ (a,d), $I_{S,aS}(\Delta t = 0)$ (b,e), and $\bar{I}_{S,aS}(\Delta t \neq 0)$ (c,f). The left panels (a–c) stand for the virtual processes before the first-order Raman peak, measured at 881 cm^{-1} Raman shift, and the right panels (d–f) stand for the virtual processes between the first-order Raman peak and the second-order Raman feature, measured at 1700 cm^{-1} Raman shift. The dashed lines indicate the dependences on the excitation laser power as follows: (a,c) linear and constant dependences; (b,e) quadratic dependences; (c,f) linear and quadratic dependences, while data fitting provides a slope of 2.1 ± 0.1 for the full data. The X and Y scales are linear in (a,d) and logarithmic in the other panels. The error bars are given by \sqrt{N} , where N is the number of counts. The error bars cannot be seen when the errors are smaller than the symbols. This experiment was performed with total accumulation time of 600 s per point, filtering only the Stokes signal with a monochromator of 26 cm^{-1} resolution.

has been published in ref. [7]. As predicted in ref. [5], $g_{S,as}^{(2)}(\Delta t = 0)$ shows an inverse excitation laser power dependence, although at very low power values it stops increasing with decreasing laser power, because the yield of Stokes-induced anti-Stokes photons becomes comparable to that of spontaneously (thermally) generated anti-Stokes photons. The $g_{S,as}^{(2)}(\Delta t = 0)$ decay predicted in ref. [5] is a simple consequence of the fact that when the number of photons increases the system tends to the classical limit where the quantum character of the event washes out.

The behavior of $g_{S,as}^{(2)}(\Delta t = 0)$ for virtual SaS is different from the real process, as shown in **Figure 5**. The $g_{S,as}^{(2)}(\Delta t = 0)$ is constant from ≈ 10 mW up to 50 mW, although the expected decay for even higher photon numbers^[5] is subtly indicated. In this range, both $I_{S,as}(\Delta t = 0)$ and $\bar{I}_{S,as}(\Delta t \neq 0)$ increase with the square of the excitation laser power, indicating that most anti-Stokes photons are indeed created in the correlated SaS scattering, and the lower counts in $\bar{I}_{S,as}(\Delta t \neq 0)$ guarantee the system is always in the quantum regime.

For excitation powers below 10 mW, $\bar{I}_{S,as}(\Delta t \neq 0)$ tends to a linear behavior with power, indicating that the spontaneous anti-Stokes emission dominates in the lower power limit. There are very few points in the low power range due to the weak signal and the difficulty to keep the laser stable for a too long time. For this reason, the exact position of the linear-to-squared power dependence is not accurately defined. However, we can argue that at 10 mW there are nearly 40 000 photons within the diamond slab, so that even at much lower powers, the pumping field can already be considered classical. The difference between the phenomenon at powers higher or lower than 10 mW is the nature of the population of the shifted modes – below 10 mW the majority of the shifted simultaneous photons is created by photonic Cooper pairs, while at higher powers the coincidental generation of pairs by two independent events becomes appreciable.

4. Concluding Remarks

Here we presented several results of $g_{S,as}^{(2)}(\Delta t = 0)$, $I_{S,as}(\Delta t = 0)$, and $\bar{I}_{S,as}(\Delta t \neq 0)$ in diamond, including the dependence on the energy Raman shift, scattering angle and excitation laser power. We hope these results will be useful for the overall understanding of the SaS correlation phenomenon, and for the search of materials with strong enough interaction energies to make this effect instrumental for applications.^[10,11]

Acknowledgments

The authors acknowledge financial support from Conselho Nacional de Desenvolvimento Científico e Tecnológico (CNPq), Brazil (307481/2013-1, 429165/2018-8, 302775/2018-8), and from the Alexander von Humboldt Foundation, Germany.

Conflict of Interest

The authors declare no conflict of interest.

Keywords

Cooper pairs, diamond, photon correlation, Raman spectroscopy

Received: April 23, 2019

Revised: May 18, 2019

Published online:

- [1] A. Jorio, A. G. Souza Filho, G. Dresselhaus, M. S. Dresselhaus, R. Saito, J. H. Hafner, C. M. Lieber, F. M. Matinaga, M. S. S. Dantas, M. A. Pimenta, *Phys. Rev. B* **2001**, 63, 245416.
- [2] A. Jorio, M. Kasperczyk, N. Clark, E. Neu, P. Maletinsky, A. Vijayaraghavan, L. Novotny, *Nano Lett.* **2014**, 14, 5687.
- [3] G. Gordeev, A. Jorio, P. Kusch, B. G. M. Vieira, B. Flavel, R. Krupke, E. B. Barros, S. Reich, *Phys. Rev. B* **2017**, 96, 245415.
- [4] D. N. Klyshko, *Sov. J. Quantum Electron.* **1977**, 7, 755.
- [5] C. A. Parra-Murillo, M. F. Santos, C. H. Monken, A. Jorio, *Phys. Rev. B* **2016**, 93, 125141.
- [6] K. Lee, B. Sussman, M. Sprague, P. Michelberger, K. Reim, J. Nunn, N. Langford, P. Bustard, D. Jaksch, I. Walmsley, *Nature Photon.* **2012**, 6, 41.
- [7] M. Kasperczyk, A. Jorio, E. Neu, P. Maletinsky, L. Novotny, *Opt. Lett.* **2015**, 40, 2393.
- [8] A. Jorio, M. Kasperczyk, N. Clark, E. Neu, P. Maletinsky, A. Vijayaraghavan, L. Novotny, *Phys. Status Solidi B* **2015**, 252, 2380.
- [9] M. D. Anderson, S. Tarrago Velez, K. Seibold, H. Flayac, V. Savona, N. Sangouard, C. Galland, *Phys. Rev. Lett.* **2018**, 120, 233601.
- [10] A. Saraiva, F. S. de Aguiar Júnior, R. M. Souza, A. P. Pena, C. H. Monken, M. F. Santos, B. Koiller, A. Jorio, *Phys. Rev. Lett.* **2017**, 119, 193603.
- [11] F. S. de Aguiar Júnior, A. Saraiva, M. F. Santos, B. Koiller, R. M. Souza, A. P. Pena, R. A. Silva, C. H. Monken, A. Jorio, *Phys. Rev. B* **2019**, 99, 100503(R).
- [12] J. Q. Shen, H. Y. Zhu, H. L. Zhu, *Laser Infrared (in Chinese)* **2002**, 32, 315.
- [13] J. Bardeen, L. N. Cooper, J. R. Schrieffer, *Phys. Rev.* **1957**, 106, 162.
- [14] M. Kasperczyk, F. S. de Aguiar Júnior, C. Rabelo, A. Saraiva, M. F. Santos, L. Novotny, A. Jorio, *Phys. Rev. Lett.* **2016**, 117, 243603.
- [15] The similarity transformation ($H' = e^{-s} H e^s$) can be applied to H_1 , where $s = \sum_{\mathbf{k}, \mathbf{q}} (\alpha_{-} c_{\mathbf{q}}^{\dagger} + \alpha_{+} c_{-\mathbf{q}}) b_{\mathbf{k}} b_{\mathbf{k}-\mathbf{q}}^{\dagger}$, with α_{\pm} chosen in order to satisfy the condition $H_1 + [H_0; s] = 0$.